Journal of the Korean Physical Society, Vol. 32, No. 2, March 1998, pp. 304∼308

The Gain Characteristics of C VI 18.2 nm Line in a Z-pinch Carbon Plasma

K. T. Lee and D. Kim

Physics Department, Pohang University of Science and Technology, Pohang 790-784

(Received 20 June 1997)

The gain dynamics of C VI Balmer-α transition at 18.2 nm in a Z-pinch carbon plasma has been studied to search for the optimal condition for the initial density and the plasma peak current. The simulation results show that there can be a significant gain of the order of 10 cm^{-1} in the optically thin case. The opacity effect is also investigated.

I. INTRODUCTION

Z-pinch plasmas have been studied for a long time. Oraevskii *et al.* [1] proposed that a Z-pinch plasma could be used as a lasing medium for extreme ultraviolet (XUV) light via either resonant photopumping or recombination pumping by radiative cooling. However, the magnetohydrodynamic (MHD) instabilities which developed during a pinch phase and broke the uniformity along the axis were considered detrimental to forming a good lasing medium. It has been known that in bounded plasmas, MHD instabilities could be suppressed. Recently, with the help of preionization, uniform plasma columns of 10- to 20-cm in length in a capillary geometry were successfully achieved and used to amplify XUV light [2–4]. Recently, Lee *et al.* [5] have shown through a detailed MHD simulation study that the adiabatic expansion after the pinch in a Z-pinch carbon plasma can lead to an adequate condition for the lasing of H-like C VI Balmer-α (n=3 to 2 transition) line at 18.2 nm.

In this paper, our extended study in search of a gain region for C VI 18.2 nm line in the parameter space of the initial gas density and the plasma peak current is presented, and a simple scaling law is discussed. The radiative trapping of Lyman-α line can seriously populate the lower lasing level (n=2), hindering population inversion between the n=3 and 2 levels. The effect of that on the gain of C VI 18.2 nm line is also presented.

II. SIMULATION MODEL

The single-fluid, two-temperature MHD equations in cylindrical geometry are used to evaluate the hydrodynamics of a Z-pinch plasma [5]. The ionization balance equation to calculate the populations of the ground state of each ionization state is incorporated. These equations include Joule heating, shock heating, Bremsstrahlung radiation, heat conduction, and magnetic field diffusion. The effects of ionization, recombination, and resonance line radiation are also considered. Axial symmetry and plasma-vacuum interface boundary conditions are adapted to this simulation.

The MHD equations in cylindrical coordinates, including the ionization balance equation, have the following forms in cgs unit:

The continuity equation (mass conservation) reads

$$\frac{d}{dt}N_i + \frac{N_i}{r}\frac{\partial}{\partial r}(rv) = 0, \tag{1}$$

where $\frac{d}{dt} = \frac{\partial}{\partial t} + v\frac{\partial}{\partial r}$, N_i is the ion density, and v is the fluid velocity in the radial direction. The momentum equation is given by

$$\begin{aligned} m_i N_i \frac{d}{dt}v &= -\frac{\partial}{\partial r}(N_e T_e + N_i T_i) - \frac{B}{4\pi r}\frac{\partial}{\partial r}(rB) \\ &\quad -2\frac{v}{r}\frac{\partial}{\partial r}\chi + \frac{\partial}{\partial r}\left(\frac{4}{3}\frac{\chi}{r}\frac{\partial}{\partial r}(rv)\right), \end{aligned} \tag{2}$$

where m_i is the ion mass, N_e the electron density, and T_e and T_i the electron and the ion temperatures, respectively. B is the magnetic field induced by the axial plasma current. The first and the second terms on the right-hand side of Eq. (2) are the thermal and the magnetic pressure, respectively; the last two terms are the shock pressure in tensor form, and χ is the shock viscosity given by [6]

$$\chi = \begin{cases} \frac{c_q}{2} l^2 m_i N_i \frac{1}{r}\left|\frac{\partial}{\partial r}(rv)\right|, & (\frac{\partial v}{\partial r}) < 0, \\ 0 & (\frac{\partial v}{\partial r}) > 0, \end{cases} \quad (\text{g cm}^{-1}\text{sec}^{-1})$$

where c_q is a constant to control the shock region. The energy balance for electrons is described by

$$\frac{d}{dt}T_e = -\frac{2}{3}T_e\frac{1}{r}\frac{\partial}{\partial r}(rv) + \frac{2}{3}\frac{1}{N_e\, r}\frac{\partial}{\partial r}\left(\kappa_{e\perp} r \frac{\partial}{\partial r}T_e\right)$$

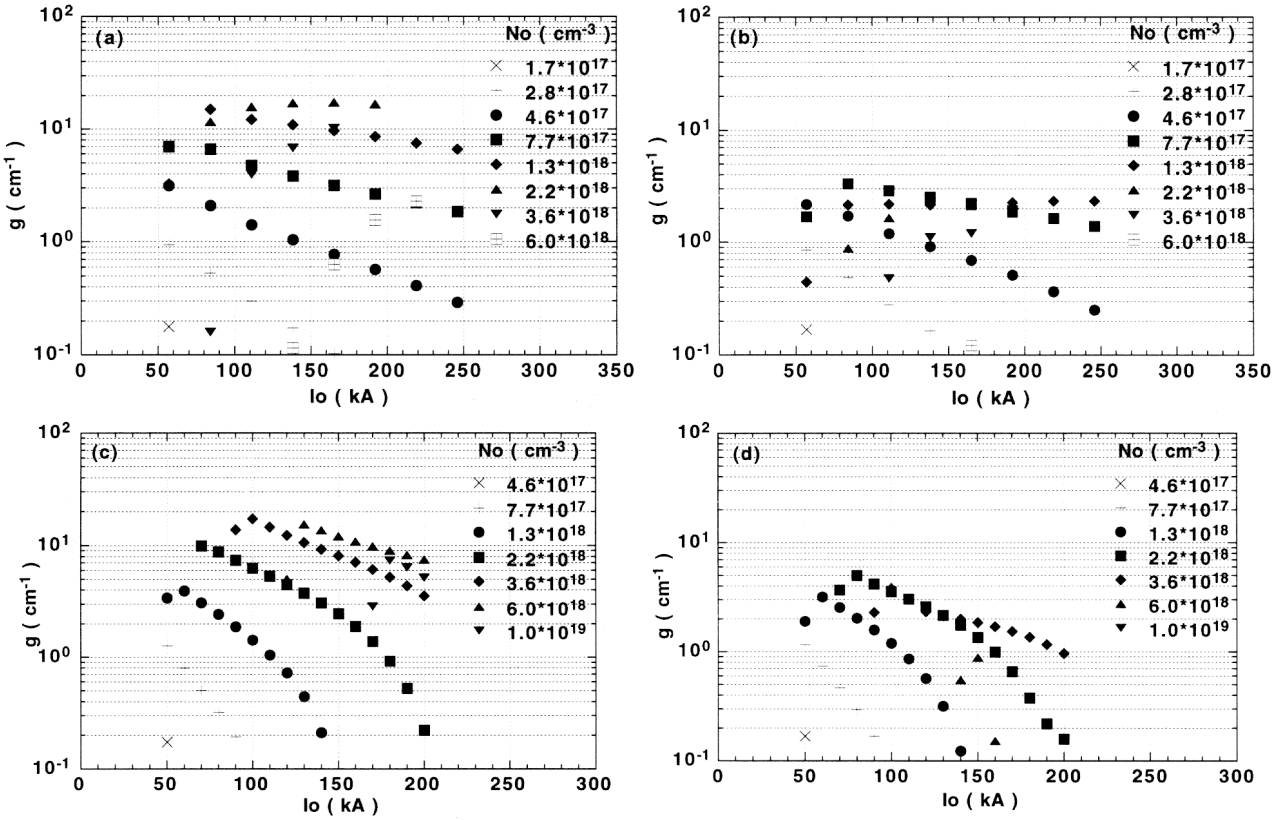

Fig. 1. Small signal gain of C VI 18.2 nm line as a function of the peak plasma current I_0 for various values of the initial plasma density N_0: (a) the optically thin case with $T/4$=100 ns and R=0.2 cm; (b) the case with the opacity $\epsilon = 0.1$ and $T/4$=100 ns, R=0.2 cm; (c) the optically thin case with $T/4$=20 ns and R=0.1 cm; (d) the case with the opacity $\epsilon = 0.1$ and $T/4$=20 ns, R=0.1 cm.

$$+\frac{2}{3}\frac{1}{N_e}(P_J - P_{brem} - P_{atom}) - P_{ei}. \qquad (3)$$

The first term is the energy loss due to the volume expansion (P_{exp_e}), the second the heat conduction (P_{cond_e}), and $\kappa_{e\perp}$ the electron heat conductivity perpendicular to the magnetic field [7]. P_J is the Joule heating given by $P_J = \eta_\perp \left[\frac{c}{4\pi}\frac{1}{r}\frac{\partial}{\partial r}(rB)\right]^2$ where $\eta_\perp$ is the plasma resistivity [8]. P_{brem} is the power loss due to Bremsstrahlung radiation [9]. The energy flows due to atomic processes include the losses due to resonance line radiation and collisional ionization and the heating due to recombination:

$$P_{atom} = P_{rad} + P_{ioniz} - P_{recomb} \text{ where}$$

$$P_{rad} = \sum_{z=1}^{nz-1} N_e N_z S_{01}^z \epsilon_z \frac{A_{10}^z}{A_{10}^z + N_e S_{10}^z},$$

$$P_{ioniz} = \sum_{z=1}^{nz-1} N_e N_z R_z \chi_z,$$

$$P_{recomb} = \sum_{z=2}^{nz} N_e N_z \alpha_z \chi_z.$$

N_z is the ion density of charge z, and A_{10}^z is the radiative decay rate of the resonance line of the z-th ionization stage having the largest A value [10]. S_{01}^z and S_{10}^z are the rate coefficients of collisional excitation and de-excitation

Table 1. Important plasma quantities are tabulated for the two sets of maximum gain parameters $(T/4, R, I_0, N_0)$. The subscript p represents the *pinch state* and g the *maximum gain*.

$T/4$(ns)	R(cm)	I_o(kA)	$N_o(10^{18}$ cm$^{-3})$	t_p(ns)	$r_{p(\mathrm{cm})}$	$T_{e,p}$(eV)	$N_{e,p}$	t_g	$T_{e,g}$	$N_{e,g}$	$g_{\epsilon=0.}(\mathrm{cm}^{-1})$	$g_{\epsilon=0.1}$
100	0.2	110	2.5	78.0	0.03	115.3	7.3	84.7	32.5	8.9	19.7	0.2
20	0.1	100	3.6	20.5	0.02	330.0	2.0	24.4	50.0	8.0	20.0	4

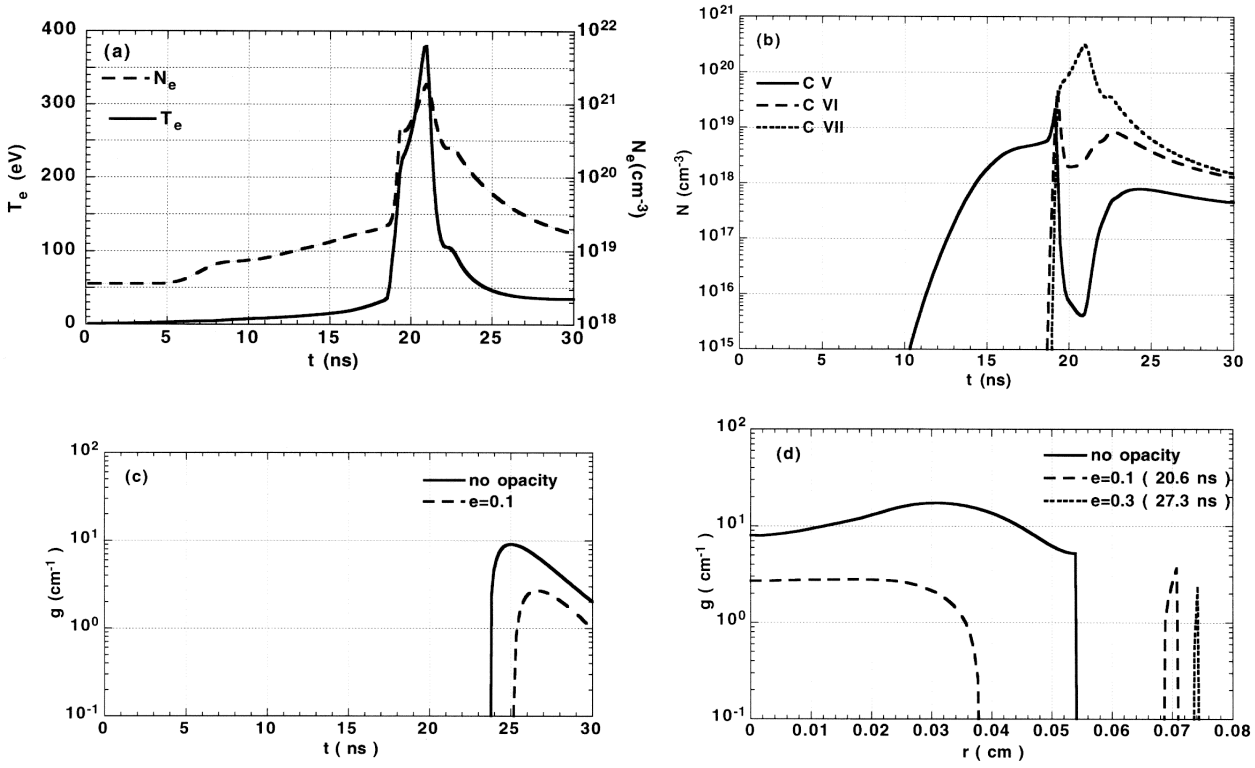

Fig. 2. For the maximum gain parameters of $T/4$=20 ns, R=0.1 cm, $I_o = 100$ kA, and $N_o = 3.6 \times 10^{18}$ cm^{-3}, the temporal variations at the axis of (a) T_e and N_e, (b) the densities of ionic stages, and (c) the small signal gain of the C VI 18.2 nm line are plotted. The spatial distributions of the gain at its maximum time are plotted in (d).

between the levels, respectively [11], and ϵ_z is their energy difference. R_z and α_z are the ionization and the recombination rate coefficients, respectively [12]. In the calculation of P_{rad}, the collisional de-excitation process is considered since it becomes significant at high density. The last term in Eq. (3), P_{ei}, is the energy equilibration between electrons and ions; *e.g.*, $P_{ei} = \frac{T_e - T_i}{\tau_{eq}}$, where τ_{eq} is the electron-ion equilibration time [9].

The energy balance for ions is governed by

$$\begin{aligned}\frac{d}{dt}T_i &= -\frac{2}{3}T_i\frac{1}{r}\frac{\partial}{\partial r}(rv) + \frac{2}{3}\frac{1}{N_i\, r}\frac{\partial}{\partial r}\left(\kappa_{i\perp} r\frac{\partial}{\partial r}T_i\right) \\ &\quad + \frac{2}{3}\frac{\chi}{N_i}\left[\frac{1}{3}\left(\frac{1}{r}\frac{\partial}{\partial r}(rv)\right)^2 + \left(r\frac{\partial}{\partial r}\left(\frac{v}{r}\right)\right)^2\right] \\ &\quad + P_{ei}, \end{aligned} \tag{4}$$

where $\kappa_{i,\perp}$ is the perpendicular ion heat conductivity [7]. The terms with χ represent the ion shock heating.

The magnetic field transport and diffusion equation reads

$$\frac{d}{dt}B = -B\frac{\partial}{\partial r}(v) + \frac{\partial}{\partial r}\left(\frac{c^2}{4\pi}\frac{\eta_\perp}{r}\frac{\partial}{\partial r}(rB)\right). \tag{5}$$

This equation is obtained using Maxwell equations and the generalized ohm's law, neglecting the time variation of the electric field [13].

The ground state population, N_z, of the z-th ionization stage is calculated using the following ionization-balance equation [11]:

$$\begin{aligned}\frac{d}{dt}N_z &= -N_e N_z\alpha_z - N_e N_z R_z \\ &\quad + N_e N_{z+1}\alpha_{z+1} + N_e N_{z-1}R_{z-1}. \end{aligned} \tag{6}$$

III. NUMERICAL METHOD

The Lagrangian scheme [14] is adopted for the numerical integration of the one-dimensional fluid equations described in the previous section. Since the integrations are performed following the fluid cells in this scheme, the continuity equation is changed to $\frac{d}{dt}\int_{\delta r} N_i r dr = 0$ and then the position of each fluid cell evolves as $\frac{d}{dt}r = v$. This Lagrangian scheme is adequate for a Z-pinch system in which a plasma is compressed by magnetic pressure. A Crank-Nicholson-type implicit scheme [14] is used to convert the differential equations into finite-difference equations. For the convenience of constructing the difference

equations, v is defined on the integral spatial-grid points and other variables on the half-integral ones. For the temporal evolution, all variables are defined on the integral temporal-grid points. To avoid numerical instability, the size of the time step, dt, is calculated at each time step using the following criterion [13]:

$$dt = c_1 Min \left\{ \left(\Delta r \sqrt{\frac{m_i N_i}{N_e T_e + N_i T_i + \frac{B^2}{4\pi}}} \right)_j \right\},$$

where the subindex j represents a spatial-grid point, c_1 is a constant used as a safety factor, and Min means the choice of the minimum value among the values in the curly brackets. The difference equations are then solved using the Thomas algorithm [14] with appropriate boundary conditions. The boundary conditions at the axis are

$$\left[\frac{\partial}{\partial r} T_e\right]_{r=0} = \left[\frac{\partial}{\partial r} T_i\right]_{r=0} = 0,$$
$$B(0) = 0,$$
$$v(0) = 0$$

due to axial symmetry. No particle moves through the plasma-vacuum interface, r_p (the outer boundary). This is represented by the following conditions [15]:

$$\left[\frac{\partial}{\partial r} T_e\right]_{r=r_p} = \left[\frac{\partial}{\partial r} T_i\right]_{r=r_p} = 0,$$
$$\left[\frac{4}{3}\chi \left(\frac{\partial}{\partial r} v - \frac{1}{2}\frac{v}{r}\right) - (N_e T_e + N_i T_i)\right]_{r=r_p} = 0.$$

The vacuum density is specified as 3.5×10^8 cm^{-3} at the outer boundary. The magnetic field at the outer boundary is calculated using an external driving current, $I(t)$, instead of solving a circuit equation:

$$B(r_p) = \frac{2}{c}\frac{I}{r_p},$$
$$I(t) = I_0 \sin(\omega t).$$

To treat the nonlinear dependence of the transport coefficients, an iteration method is adopted. The evaluation of the ionization balance equations is carried out using the method suggested by Carolan and Piotrowicz [16] which involves an eigenvalue problem.

The collisional-radiative model is used to calculate the populations of the excited levels of H-like C VI under a quasi-steady state. For this calculation, 20 levels are included. Among them, the populations of the upper 5 levels are obtained under local thermodynamic equilibrium. The small signal gain of H-like C VI 18.2 nm line is calculated with Doppler broadening [11].

IV. RESULTS AND DISCUSSION

For two different sets of the quarter-period of the plasma current ($T/4$) and the initial plasma radius (R), the gain of C VI 18.2 nm line is calculated for different initial plasma densities (N_o) and peak plasma currents (I_o). Figure 1 shows the variation of the gain for the two sets of $T/4$ and R. First of all, the result shows that the gain region is rather wide. Once the gain is obtained for a certain set of parameters, it is easy to look for another set of parameters. The simulation shows that a high initial density is required for the gain, $N_o \simeq 10^{18}$ cm^{-3}, which corresponds to a pressure of 30 Torr. This is very high compared with the recent experimental conditions: 0.3 Torr for Ne-like Argon [3] and 0.15 Torr for Li-like Oxygen [4]. It is even high when compared with the suggested initial density of 0.75 Torr for H-like carbon [17]. The peak current for maximum gain is about three times larger than those in the above experiments, but a quarter of the value of 400 kA for a 70-ns pinch time suggested by Hartmann *et al.* [17]. The important quantities of a Z-pinch plasma for maximum gain parameters are tabulated in Table 1.

To reach a gain condition in the electron-collisional recombination scheme, the electron temperature should be decreased faster than the recombination of C VII ions to C VI ions. Figure 2 shows the dynamics of the plasma at the axis for the maximum gain parameters of $T/4 = 20$ ns and $R = 0.1$ cm. For these parameters, the cooling rate is $\simeq 2.1 \times 10^9$ s^{-1}, mainly due to adiabatic expansion after the high-density, high-temperature pinch [5], and the recombination rate is $\simeq 1.6 \times 10^9$ s^{-1}, which satisfies the pumping requirement by recombination. Hence, by the adiabatic expansion alone, the plasma can reach a supercooled state, contrary to the results of a previous analysis [1]. The electron temperature and the density at the time of maximum gain are 50 eV and 8×10^{19} cm^{-3}, which are less relaxed compared with the analysis of Elton [11]. These parameters give 2.7 for the collision-limit, adequate for a population inversion between the n=3 and 2 levels. The gain increases very rapidly up to 20 cm^{-1} and is sustained for about 10 ns. The spatial distribution has its maximum off-axis.

The effect of the reabsorption of Lyman-α line is investigated for the maximum gain parameters (see Figs. 1(b) and (d)). The escape probability method, including the Doppler shift due to the large velocity gradient in the plasma, is adopted [18]. Following the suggestion of Pert [19], an anomaly factor(ϵ) is introduced to vary the reabsorption effect:

$$\tau_{eff} = \epsilon \tau_{actual}, \tag{7}$$

where τ_{actual} is optical depth calculated by the method of Shestakov and Eder [20] or Lee *et al.* [18]. Since the effect of reabsorption of the resonance lines on the hydrodynamics is negligible [5], it is considered only for the calculation of the populations of the excited levels.

The reabsorption effect with $\epsilon = 0.1$ reduces the maximum gain by a factor of 4 and changes the maximum gain parameters. For a low density, the effect is

negligible, but as the initial density increases, this effect becomes significant, eventually removing the gain at $N_o = 10^{19}$ cm^{-3}. Actually, this effect shrinks the gain region in the parameter space of the initial density and the peak plasma current because for high initial density, the gain appears at a high peak plasma current. Because the maximum gain parameter is changed by the opacity, an investigation is required to find the actual optimized condition. The opacity effect on the gain dynamics can be seen from Figs. 2(c) and (d). With increasing opacity, not only is the gain reduced and appears later but also its region becomes narrow. For $\epsilon = 0.3$, the gain appears only at the plasma boundary but this may be difficult to observe in an experiment due to refraction. The opacity also flattens the spatial distribution of the gain.

A simple but useful scaling law for the gain region in the parameter space can be obtained using the condition of $t_p \propto T$, where t_p is the pinch time given by the snowplow model. From law for the scaling of the electron density to the atomic number Z, $N_e \propto Z^7$ cm^{-3} [11], the initial density can be written as $N_o \propto Z^6$. Then, the scaling formula is given as

$$\frac{TI_o}{R^2} \propto A^{\frac{1}{2}} Z^3 \tag{8}$$

where A is atomic weight. Hence, $\frac{TI_o}{R^2}$ is constant for a given atomic species. For two sets of the maximum gain parameters, Eq. (8) yields 11 and 8, respectively, justifying reasonably the above scaling law. Even if there are some discrepancies, the equations given above, Eq. (8) yields a very useful estimate of the gain region. The relationship in Eq. (8) gives the scaling with Z, which can be used to design an experimental device for different elements or different wavelengths.

V. CONCLUSIONS

An extended study to search for the gain region for C VI 18.2-nm line in the parameter space of the initial gas density and the plasma peak current has been carried out for two different sets of values for the quarter-period of the plasma current ($T/4$) and the initial plasma radius (R). The calculation of the gain has been performed for different initial plasma density (N_o) and the peak plasma current (I_o). There can be a significant gain of the order of 10 cm^{-1} in the optically thin case. With increasing opacity, not only is the gain reduced and delayed but also its region becomes narrow. On the positive side, the reabsorption effect flattens the spatial distribution of the gain.

ACKNOWLEDGMENTS

This work has been supported in part by the Pohang University of Science and Technology/Basic Science Research Institute special fund in 1996, the Basic Science Research Institute Program, Ministry of Education, 1995 (Project No. BSRI-95-2439), and the Korea Science and Engineering Foundation (Contract No. 951-0205-017-2).

REFERENCES

[1] A. N. Oraevskii, O. G. Semenov and B. N. Chichkov, Sov. J. Quantum Electron. **17**, 1274 (1987).
[2] H. J. Shin, D. E. Kim and T. N. Lee, Phys. Rev. **E50**, 1376 (1994).
[3] J. J. Rocca, V. Shlyaptsev, F. G. Tomasel, D. D. Cortazer, D. Hartshorn and J. L. A. Chilla, Phys. Rev. Lett. **73**, 2192 (1994).
[4] T. Wagner, E. Eberl, K. Frank, W. Hartmann, D. H. H. Hoffmann and R. Tkotz, Phys. Rev. Lett. **76**, 3124 (1996).
[5] K. T. Lee, S. H. Kim, D. Kim and T. N. Lee, Phys. Plasmas **3**, 1340 (1996).
[6] R. L. Bowess and J. R. Wilson, *Numerical Modeling in Applied Physics and Astrophysics* (Wones and Bartlett, Boston, 1991), Chap. 4.
[7] D. Düchs and H. R .Griem, Phys. Fluids **9**, 1099 (1966).
[8] S. I. Braginskii, *Review of Plasma Physics*, edited by A. M. A. Leontovich (Consultants Bureau, New York, 1965), Vol. 1, p. 216.
[9] Lyman Spitzer, *Physics of Fully Ionized Gases*, 2nd ed. (Wiley, New York, 1962), p. 148.
[10] W. Wiese, M. Smith and B. M. Glennon, *Atomic Transition Probabilities* (U.S. Goverment Printing Office, Washington, D.C., 1966), Vol. I.
[11] R. C. Elton, *X-ray Lasers* (Academic, New York, 1990), Chaps. 2 and 4.
[12] R. W. P. McWhirter, *Plasma Diagnostic Techniques*, edited by R. H. Huddlestone and S. L. Leonard (Academic Press, New York, 1965), Vol. 21, Chap. 5.
[13] N. H. Burnett and A. A. Offenberger, J. Appl. Phys. **45**, 2155 (1974).
[14] R. D. Richtmyer and K. W. Morton, *Difference Methods for Initial-Value Problems*, No. 4 (Interscience, New York, 1967).
[15] V. F. D'yachenko and V. S. Imshennik, *Review of Plasma Physics*, edited by A. M. A. Leontovich (Plenum, New York, 1970), Vol. 5, p. 462.
[16] D. G. Carolan and V. A. Piotrowicz, Plasma Phys. **25**, 1065 (1983).
[17] W. Hartmann, H. Bauer, J. Christiansen, K. Frank, H. Kuhn, M. Stetter, R. Tkotz and T. Wagner, Appl. Phys. Lett. **58**, 2619 (1991).
[18] Y. T. Lee, R. A. London, G. B. Zimmerman and P. L. Hagelstein, Phys. Fluids **B2**, 2731 (1990).
[19] G. J. Pert, *X-ray Lasers 1990*, edited by G. J. Tallent (Institute of Physics, New York, 1990), p. 143.
[20] A. I. Shestakov and D. C. Eder, J. Quant. Spectrosc. Radiat. Transfer **42**, 483 (1989).